LIMNOLOGY and OCEANOGRAPHY

ASLO

Limnol. Oceanogr. 71, 2026, e70475

doi: 10.1002/lno.70475

REPORT

Phosphate modulates elemental and macromolecular composition of unicellular nitrogen-fixing cyanobacteria

Sing-how Tuo [1,2*] **Ying-Yu Hu** [1] **Andrew J. Irwin** [3] **Michael J. Follows** [4] **Zoe V. Finkel** [1]

[1]Department of Oceanography, Dalhousie University, Halifax, Nova Scotia, Canada; [2]Department of Oceanography, National Sun Yat-sen University, Kaohsiung, Taiwan; [3]Department of Mathematics and Statistics, Dalhousie University, Halifax, Nova Scotia, Canada; [4]Department of Earth, Atmospheric and Planetary Science, Massachusetts Institute of Technology, Cambridge, Massachusetts, USA

Abstract

The C : N : P of nitrogen-fixing cyanobacteria regulates phosphate-limited nitrogen fixation in the ocean yet the causes and range in variation C : N : P is not well constrained. Here we quantify the C : N : P and underlying macromolecular composition of *Crocosphaera*. *Crocosphaera* is a nitrogen-fixing cyanobacterium that substantively contributes to elemental biogeochemistry in the (sub)tropical oceans. We observed variation in C : N : P and macromolecular composition over the photoperiod, across two different sized phenotypes and with phosphate concentration. In both phenotypes, C : N is ~ 1.3-fold higher in the day than the night due to increasing carbohydrate in the smaller phenotype and increasing lipid in the larger phenotype during the day and increasing protein in both phenotypes at night. Detectable levels of surface adsorbed phosphorus were only observed at night. The two sized phenotypes differed in macromolecular allocation: the smaller phenotype had a higher proportion of carbon to DNA, RNA, and chlorophyll *a* while the larger phenotype was higher in lipids relative to carbohydrates. The largest variation in C : N : P arose with changes in phosphate concentration. Decreasing phosphate in the media from 50 to 0.5 μM induced a 27-fold decrease in cellular P, increasing molar N : P from ~ 2 to between 41 and 64 and C : P from ~ 15 to between 335 and 484 across the phenotypes. Much of these changes can be attributed to changes in polyphosphate content and secondarily DNA content. The accumulation and storage of polyphosphate under higher phosphate concentrations could temporarily increase *Crocosphaera*'s capacity to fix nitrogen when phosphate is scarce.

The global ocean's fixed nitrogen inventory is set by the balance between nitrogen fixation, primarily by cyanobacteria, and denitrification by anaerobic bacteria and archaea (Falkowski 1997). Theory and numerical simulations suggest that the integrated nitrogen fixation by N_2-fixing cyanobacteria is strongly controlled by nutrient availability, specifically the relative supply of iron and the excess phosphorus left behind by the non-Redfield N : P nutrient uptake of non-N_2-fixing phytoplankton (Dutkiewicz et al. 2012; Mills and Arrigo 2010; Weber and Deutsch 2014). N_2-fixing cyanobacteria have been assumed to have a high N : P stoichiometry (Mills and Arrigo 2010), but experimental evidence shows that the particulate N : P ratio of N_2-fixing cyanobacteria varies considerably across taxa and environmental conditions from a low of 1.5 to > 150 (Masuda et al. 2013; Mulholland et al. 2002). There are many hypothesized reasons for these variations. On physiological scales, acclimation to low light requires N-rich photosynthetic protein and high growth requires both N-rich biosynthetic protein and high RNA content (Inomura et al. 2020); when phosphorus is plentiful it may be stored, decreasing N : P. The diel forcing of the day-night cycle also induces variation in macromolecular and elemental stoichiometry with changes in photosynthetic and nitrogen fixation rates (Dron, Rabouille, Claquin, Chang, et al. 2012; Dron, Rabouille, Claquin, Le Roy, et al. 2012). Over longer time scales, adaptation to specific environmental regimes may lead to phenotypes with distinct macromolecular

*Correspondence: stuo@mail.nsysu.edu.tw

Associate editor: Miriam Gerhard

and elemental stoichiometries. For example, phenotypes with different cell sizes will influence mass-specific nutrient and gas diffusion rates, the fraction of total biomass accounted for by the cell wall (which can be especially N- and C-rich), and when cells are especially small, a higher proportion of cell mass can be associated with P-rich membranes and DNA content (non-scalable components) (Raven 1994). Many factors may lead to nitrogen-fixing cyanobacteria having high N : P ratios relative to the Redfield ratio and other phytoplankton groups, but the macromolecular basis and extent of N : P differences and the variability across nitrogen-fixing species and phenotypes is not well documented.

Crocosphaera watsonii is a widespread N_2-fixing cyanobacterium found in the tropical and subtropical oceans, where *Crocosphaera* has been estimated to contribute 54–100% of bulk N_2 fixation rates (Benavides et al. 2022; Zehr et al. 2001). *Crocosphaera* is a unicellular cyanobacterium, so to reduce nitrogenase inactivation from oxygen exposure produced from photosynthesis during the day, it fixes nitrogen at night, driving diel patterns in C : N and glycogen content (Dron, Rabouille, Claquin, Le Roy, et al. 2012; Saito et al. 2011). *Crocosphaera watsonii* has two main sized phenotypes: the large-cell phenotype is often 4–6 μm in diameter (Webb et al. 2009; Zehr et al. 2001) and the small-cell phenotype is < 4 μm in diameter (Bench et al. 2013; Webb et al. 2009; Zehr et al. 2001). In the North Pacific, the small-cell phenotype is more abundant than the large-cell phenotype in the upper water column, while the large-cell phenotype is often more abundant lower in the water column (Bench et al. 2016; Wilson et al. 2017). Cell size may influence the physiology, biochemistry, and ultimately the biogeography and depth distribution of *Crocosphaera watsonii*. Smaller cells have higher surface area to volume ratios that provide them with a competitive advantage for light and nutrients—perhaps explaining the higher abundance of the small-cell phenotype in the nutrient-depleted upper surface of the subtropical oceans. Here we quantify differences in C : N : P and macromolecular content across two size phenotypes of *Crocosphaera* in the light and dark period. In addition, we examine the sensitivity of C : P and N : P in the two *Crocosphaera* size phenotypes to phosphate availability.

Materials and methods

Strains and culture condition

Two strains of *Crocosphaera*, WH8501 (small-cell phenotype) and WH0005 (large-cell phenotype), were isolated from the tropical South Atlantic (28°S, 48°W) and North Pacific (22°N, 158°W) Oceans, respectively (Bench et al. 2013). Cultures were grown in 2.4-L acid-washed polycarbonate bottles with 2 L of combined nitrogen-free (nitrate, nitrite, and ammonium were under the detection limit) YBCII culture medium (Y. Chen et al. 1996) with 50-μM phosphate concentration (original recipe). The phosphate concentration was decreased to 0.5 μM for a lower phosphate experiment. For all experiments, the cultures were kept in an incubator with temperature controlled at 26°C and light intensity of 50 μmol quanta m^{-2} s^{-1} on a 12 : 12 h light : dark square wave cycle.

For the acclimation phase and the treatment evaluation, we monitored cell density (cells mL^{-1}) and cell diameter (D, μm) every 2 d till harvest using a Multisizer 3 particle counter (Beckman Coulter) equipped with a 50-μm aperture tube and pre-calibrated by using a standard calibrator (Beckman Coulter CC Size Standard L5) and following the user manual; the low detection limit (L-LOD), low quantification limit (L-LOQ), and high detection limit (H-LOD) for cell diameter estimation were 0.02, 1.5, and 30 μm, respectively. Cell volume (V, μm^3), cell surface area (SA, μm^2), and the ratio of $SA : V$ are calculated by the formulae for the volume and the surface area of a sphere.

For acclimation, cultures were grown semi-continuously for a minimum of 15 generations before the start of the experiment. Cultures were transferred into fresh culture medium before cell density reached the early stationary growth phase (1200×10^3 and 600×10^3 cells mL^{-1} for WH8501 and WH0005, respectively) based upon preliminary culture experiments (Supporting Information Fig. S1). Bacterial contamination was monitored with a BD Accuri C6 flow cytometer according to Marie et al. (2005) and was well-controlled. At cell harvest, bacteria density in the WH8501 and WH0005 bottles was $74.8 \pm 6.98 \times 10^3$ ($n = 8$) and $9.98 \pm 2.02 \times 10^3$ cells mL^{-1} ($n = 8$), respectively. Assuming contaminating bacteria have 350 fg C $cell^{-1}$, 90 fg N $cell^{-1}$, and 17 fg P $cell^{-1}$ (Fagerbakke et al. 1996), we estimate that bacteria biomass contributed only 0.34% ± 0.18% C, 0.58% ± 0.26% N, and 0.09% ± 0.04% P (across strains, $n = 16$).

Sampling strategy

Crocosphaera is known to temporally separate photosynthesis (during the light period) and nitrogen fixation (mostly limited to the night), impacting cellular C and N content and C : N ratios. To quantify the elemental and macromolecular composition of the two phenotypes between day and night, we therefore used a 2 × 2 factorial design: eight replicate polycarbonate bottles each phenotype, four for the harvest 12 h into the dark period (D12) and four bottles to harvest 12 h after the initiation of the light period (L12). For each element or macromolecular analysis, three subsamples for technical replicates were collected from each bottle at harvest. Before the harvest, each phenotype was grown under batch conditions for 8 d (WH8501, initial 400×10^3 cells mL^{-1} at the inoculation) or 10 d (WH0005, initial 45×10^3 cells mL^{-1}) after the 15-generation acclimation. The specific growth rate (d^{-1}) of the culture was calculated as the slope of the least squares regression line of natural log cell density as a function of time (d) using LINEST and LN in Microsoft Excel. Cultures were considered to be in exponential phase when abundance was between 400×10^3 and 1200×10^3 cells mL^{-1} for WH8501 and between 45×10^3 and 600×10^3 cells mL^{-1} for WH0005

(Supporting Information Fig. S1). Four bottles in the WH8501 culture had entered early stationary phase (2 at D12 and 2 at L12); as their specific growth rate at the time of harvest was approaching zero, although the differences in cell dimensions and elemental and macromolecular compositions between exponential and these stationary growth phase samples were not significant (Supporting Information Tables S1–S3); therefore, data acquired from these four stationary bottles were omitted from further analyses.

We performed an additional experiment using 0.5 μM phosphate to examine the effect of phosphate supply on C : N : P ratios. Each culture was acclimated for a minimum of 51 generations (to ensure P stores acquired in the original medium with higher phosphate concentrations had been consumed) before the experiment. Each phenotype was grown in three replicate polycarbonate bottles and harvested only at D12 for particulate elemental analyses, with three technical replicates of each bottle. No macromolecular samples were taken from the low phosphate experiment.

Dissolved nutrient and particulate elemental analyses

Dissolved nitrate, nitrite, ammonium, and phosphate from the culture media were filtered through GF/F precombusted filters (450°C for 4 h, approximately 0.3 μm after combustion) (Nayar and Chou 2003) at the harvest. Dissolved nutrient samples were stored at −20°C until analysis using a Skalar Autoanalyzer as specified by the manufacturer, with L-LOD and L-LOQ of 0.05 and 0.16 μM for nitrate, 0.01 and 0.02 μM for nitrite, 0.06 and 0.19 μM for ammonium, as well as 0.01 and 0.14 μM for phosphate.

For total particulate carbon and nitrogen analyses, samples and media blanks were collected on precombusted GF/F filters (450°C for 4 h), dried at 60°C for 48 h, and pelleted in pressed D5055 (Isomass Scientific) tin capsules. The packed samples were analyzed using a UNICUBE Vario MICRO cube elemental analyzer.

Particulate phosphorus samples were collected on 0.2-μm pore-sized polycarbonate membrane filters. To differentiate between cellular phosphorus and surface adsorbed phosphorus (ads-P), two samples were taken; one set was rinsed with un-enriched artificial seawater to provide an estimate of total particulate phosphorus and the other set was rinsed with an oxalate reagent (Tovar-Sanchez et al. 2003) to remove ads-P and provide an estimate of cellular phosphorus. Both types of samples were dried with 200 μL 0.17 M $MgSO_4$, combusted at 800°C for 9 h (Hu, Irwin, and Finkel 2022), and then digested by 0.2 M HCl at 90°C for 30 min (Solórzano and Sharp 1980). Phosphorus was quantified using a modified ammonium molybdate method (P. Chen et al. 1956), scaled down for a microplate-based assay, using KH_2PO_4 as a standard (Hu, Irwin, and Finkel 2022). Adsorbed P was calculated as the difference between total particulate phosphorus and cellular phosphorus.

Macromolecular analyses

Samples for DNA, RNA, and protein (total cellular protein plus any adsorbed transparent exopolymeric particle protein) were collected on 0.2-μm pore-sized polycarbonate membrane filters, while samples for chlorophyll *a* (Chl*a*), carbohydrates (total cellular carbohydrates plus any adsorbed transparent exopolymeric particle carbohydrates), lipids, lipid-associated phosphorus (lipid-P), and polyphosphate (poly-P) were collected on pre-combusted GF/F filters (450°C for 4 h). Samples for macromolecular analyses were immediately flash frozen in liquid nitrogen and then stored at −80°C until analysis. Prior to analysis, all the samples (except for Chl*a*) were freeze-dried (FreeZone 2.5 L −50°C Benchtop Freeze Dryers, LABCONCO) for 4 h.

Cellular DNA and RNA quantification followed a modified method from Berdalet et al. (2005) method, as described in Hu and Finkel (2023c). Briefly, the samples were broken by bead milling (FastPrep Lysing Matrix D, 1.4-mm zirconium-silicate spheres) in an extraction buffer that included a 20% *n*-lauryl sarcosine sodium salt solution (Sigma-Aldrich L744), 5 mM Tris (pH 8.0, Fisher AAJ60080AK), and 0.5 mM ethylenediaminetetraacetic acid (Bioshop EDT333.100). Bead milling was performed using a FastPrep-24 5G bead beater (four times for 30 s at 6.5 m s^{-1}, with samples placed on ice for 90 s between each round). The homogenate was vortexed at room temperature for 1 h and then centrifuged (Eppendorf Centrifuge 5424R) at 13,000 rpm for 5 min. The supernatant was treated with RNase (Sigma-Aldrich R6513), DNase (Bioshop DRB002.10), and RNase plus DNase, and stained with SYBR Green II (Thermo Fisher S7564). DNA and RNA contents were then determined by SYBR Green II fluorescence, measured in a 96-well opaque black microplate using a Varioskan LUX with corrections applied based on the background fluorescence present after nuclease treatment. DNA was quantified against a Type IX calf thymus DNA standard (Sigma# D4522) and RNA was quantified against an *Escherichia coli* ribosomal RNA standard (Ambion#7940).

Chl*a* samples were extracted directly by saturated magnesium carbonate-buffered 90% (v/v) acetone: dimethyl sulfoxide = 3:2 solvent for 30 min in the dark (Shoaf and Lium 1976), and then measured by a 10-AU fluorometer (Turner Designs).

Total protein was extracted and precipitated and then quantified (Hu, Lord, and Finkel 2022a, 2022b). In brief, protein samples were homogenized in Lysing Matrix D tubes (FastPrep, 1.4-mm zirconium-silicate spheres) and extracted by protein extraction buffer (Ni et al. 2017). Bead milling was performed four times for 1 min at 6.5 m s^{-1} using a FastPrep-24 5G (MP Biomedicals), with samples placed on ice for 1 min between each round of bead milling to prevent degradation by heating. The crude protein was subsequently precipitated by the chloroform–methanol method and dried in a vacuum desiccator. Precipitated protein was then redissolved in 95 μL Tris buffer (pH 8.0) with 5 μL 20% sarcosine (Sigma Aldrich

61747), and measured using a Pierce bicinchoninic acid assay and microplate reader (Varioskan LUX, Thermo Scientific) with bovine serum albumin as a standard; the L-LOD, L-LOQ, and H-LOD were 0.012, 0.035, and 1.000 mg mL^{-1}.

Carbohydrates, lipids, and the phosphorus content associated with lipids (lipid-P) were all measured from the same sample filter following the method of Hu and Finkel (2022), Hu and Finkel (2023b), and Hu et al. (2024). Samples were first vortexed in 9-M H_2SO_4 for 15 s and then diluted to a final H_2SO_4 molarity of 1.6 M and hydrolyzed for 3 h at 90°C. Chloroform (2 mL) was added into the hydrolysate and then the mixture was centrifuged at 3200 rpm for 5 min at room temperature. The supernatant was transferred and then alkalinized by adding 12 M NaOH to the hydrolysate; the ratio of $[H^+]$ from the hydrolysate to $[OH^-]$ from NaOH was 0.82. Carbohydrates were measured using the alkalinized hydrolysate and a modified version of the 2,4,6-tri(2-pyridyl)-s-triazine method (Myklestad et al. 1997) using 595 nm in a microplate and glucose as the standard, with L-LOD, L-LOQ, and H-LOD of 5, 16, and 10,000 ng C mL^{-1}, respectively (Hu et al. 2024). Methanol (1 mL) was added to the residue from the carbohydrates hydrolysis, vortexed, and sonicated to extract lipids into the organic phase. A 0.88% KCl solution was added to the organic layer followed by vortexing and then centrifuging at 3200 rpm for 5 min at room temperature. The lower organic phase was transferred to a storage vial, and the extract was dried under a stream of N_2 gas (< 2 psi). The dried extract was redissolved using 5 mL of chloroform and divided into two portions. Each portion was dried under a stream of N_2 gas. One portion was measured using the acid-dichromate method (Pande et al., 1963) in a microplate; absorbance was read at 348 nm instead of the commonly used 440 nm for a much higher sensitivity, and glyceryl tripalmitate was used as standard; the L-LOD, L-LOQ, and H-LOD were 6, 18, and 100 μg $assay^{-1}$, respectively. The other portion was dried with 200-μL 0.17 M $MgSO_4$ and then combusted at 650°C for 9 h. The ash was digested by 0.5 mL 0.2 M HCl at 90°C for 30 min. The phosphate was then quantified using the ammonium molybdate method (P. Chen et al. 1956), modified for a microplate reader (Varioskan LUX multimode), using KH_2PO_4 as standard; the L-LOD, L-LOQ, and H-LOD were 1.1, 3.3, and 49 μM, respectively. The final phosphorus associated with lipids (lipid-P) was corrected by a factor of 0.8 due to the incomplete recovery of phospholipids combusted at 650°C (Hu and Finkel 2023b).

Intracellular polyphosphate (poly-P) was measured using a modified version of the 4′,6-diamidino-2-phenylindole method as described in Hu and Finkel (2023a). Briefly, Tris buffer (20 mM, pH = 7) was added to freeze-dried samples, sonicated, and kept in a boiling water bath for 5 min. This extraction process was repeated 5–7 times; the extracts were pooled and centrifuged at 12,000 rpm for 5 min. After being treated by proteinase K (Fisher Scientific BP1700-500), RNase A and T1 (Fisher Scientific AM2288), and TURBO DNase (Fisher Scientific AM2239), part of the extract was amended by a standard solution of polyP-45 (Sigma Aldrich S4379). 4′,6-Diamidino-2-phenylindole was added to both the extract and amended extract and loaded into an opaque black microplate. A lid with a black film was used to avoid photobleaching 4′,6-diamidino-2-phenylindole–stained samples and then removed before the microplate measurement.

Data analyses

The C, N, P cellular content (Q_C, Q_N, and Q_P, fmol $cell^{-1}$) attributable to each macromolecular pool was calculated using the average C : N : P stoichiometry for each macromolecule reported by Geider and La Roche (2002) and Sterner and Elser (2003).

To assess the difference in cell dimensions, elemental and macromolecular composition between phenotypes and between the light and dark photoperiods under 50 μM phosphate, a two-way ANOVA with Type II or Type III sum of square was applied for the unbalanced dataset. When the interaction effect of phenotype × photoperiod was significant ($p < 0.05$), a Student's *t*-test was applied for WH0005 to assess the difference between the photoperiods in WH0005. Student's *t*-tests were also applied to assess the difference of specific growth rate between phenotypes and the difference in cell dimensions and elemental composition between phenotypes in the low phosphate experiment. All data are presented as means with one standard deviation. All the statistical analyses were performed using IBM SPSS Statistic 28.0.0.0 (190).

Results

Cell dimensions and growth rate

WH8501 had significantly smaller cell diameter and volume than WH0005. Cell diameter and volume are larger in the light as compared to the dark period (Fig. 1a,b; Supporting Information Tables S4, S5). Under 0.5 relative to 50 μM phosphate, cell diameter and volume decrease in WH8501 but increase in WH0005. Accordingly, $SA : V$ showed opposite trends between phenotypes and between periods (Fig. 1c). Under 50 μM phosphate, the small-cell phenotype WH8501 grew significantly faster (0.12 ± 0.02 d^{-1}, $n = 8$) than the large-cell strain WH0005 (0.09 ± 0.01 d^{-1}, $n = 8$) ($t = 3.59$, df = 14, two-sided $p < 0.01$, as the variance between strains was not significantly different, $F_{7,7} = 4.50$, $p > 0.05$) (Supporting Information Note S1). During this experiment, combined nitrogen was below detection limits and phosphate concentration was reduced 63% (± 6%, $n = 8$) and 21% (± 4%, $n = 8$) at the time of harvest relative to the initial culture media for WH8501 and WH0005, respectively. Under 0.5 μM phosphate, the specific growth rate of both phenotypes increased and was not significantly different from one another (Supporting Information Table S5 and Note S1).

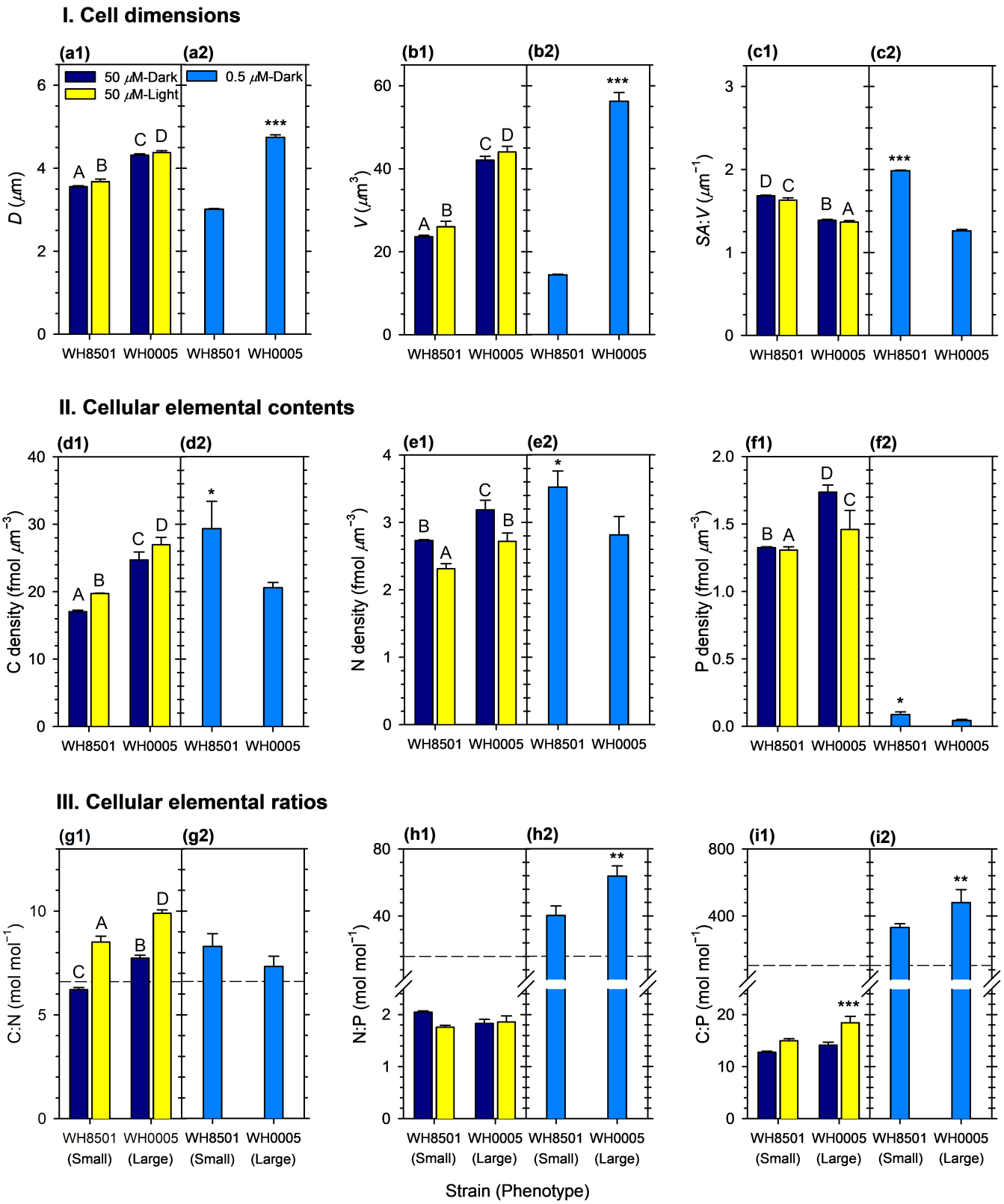

Fig. 1. Legend on next page.

Elemental ratios

WH0005 had significantly higher cellular carbon, nitrogen, and phosphorus (Q_C, Q_N, and Q_P) than WH8501. Both phenotypes exhibit relatively stable Q_C and Q_N regardless of phosphate concentration (Supporting Information Tables S4, S5). In the light vs. the dark period, the C density (fmol μm^{-3}) is 13% higher, N density is 18% lower, and P density is 10% lower (Supporting Information Table S4). Under 0.5 μM phosphate, Q_P and P density decreased 27-fold in both strains, C and N density increased in WH8501, and no significant change in C or N density was observed in WH0005 relative to 50 μM phosphate (Fig. 1d–f).

The C : N of the tested *Crocosphaera* strains ranges between 6.2 and 9.9, with most of the variability associated with the phenotype and photoperiod (Fig. 1g). C : N was significantly ($\sim$ 37%) higher in the light vs. the dark period for both phenotypes. The large-cell phenotype had $\sim$ 20% higher C : N than the small-cell phenotype under 50 μM phosphate, whereas the ratio was comparable between phenotypes under 0.5 μM phosphate.

N : P ranges from 1.8 to 64 and C : P ranges from 13 to 484 across strains, time of day, and with phosphate concentration in the media (Fig. 1h–i). By far most of the variability in N : P and C : P is due to phosphate concentration in the media. Under 50 μM phosphate, N : P ranges from 1.8 to 2.1 and C : P ranges from 12.9 to 18.6, and are similar in value across the phenotypes, and over the light and dark period. Under 0.5 μM phosphate, N : P and C : P are 1.6- and 1.4-fold higher in WH0005 relative to WH8501, respectively.

Macromolecular composition

WH0005 had significantly higher cellular macromolecular density (mass per cell) for all the macromolecules assayed (Supporting Information Table S6). Furthermore, WH0005 is especially higher in lipids, protein, lipid-P, and polyphosphate after cell volume normalization, and lower in DNA per cell volume, resulting in higher RNA : DNA and lipids : carbohydrates compared with WH8501 (Supporting Information Tables S6, S7). WH8501 had higher DNA (1.5-fold) and Chl*a* per cell volume (1.3-fold) compared to WH0005, although Chl*a* per cell area was comparable across the phenotypes. Both phenotypes showed diel patterns in carbohydrates, lipids, protein, and ads-P content (Supporting Information Tables S6, S7). Carbohydrates, lipids, and surface ads-P content are higher in the light period and protein content is higher in the dark period. In the large-cell phenotype, RNA content (both per cell and volume normalized) was also higher in the dark than the light period and RNA : DNA was higher in the dark in both phenotypes. The other macromolecules (per cell), including DNA, Chl*a*, lipid-P, and poly-P, were comparable across the light–dark cycle in both phenotypes.

Macromolecular allocation to cellular C, N, and P

The macromolecules such as protein, carbohydrates, lipids, RNA, DNA, Chl*a*, and polyphosphate and ads-P account for > 90% of cellular carbon, > 86% of cellular nitrogen, and > 90% of cellular phosphorus in *Crocosphaera* (Fig. 2; Supporting Information Table S8). Protein, carbohydrates, and lipids account for most of cellular carbon; protein accounts for most of cellular nitrogen; and polyphosphate accounts for the most of cellular phosphorus (Fig. 2). WH8501 allocates a higher proportion of its carbon to DNA, RNA, Chl*a*, carbohydrates (in the day), and a lower proportion to lipids relative to WH0005 (Fig. 2a–e). WH8501 allocates more of its nitrogen to DNA, RNA (in the day), and Chl*a*, but less of its nitrogen to protein than WH0005 (Fig. 2g–j). In addition, WH8501 allocates more of its phosphorus to DNA and RNA but less to phospholipids than WH0005 (Fig. 2k–m).

Carbon allocation to carbohydrates, lipids, protein, RNA, DNA, and Chl*a* varies over the light–dark cycle. Carbon allocation to protein, DNA, RNA, and Chl*a* is higher in the dark period, while allocation to carbohydrates (for WH8501) is higher in the light period (Fig. 2a–f). Nitrogen and phosphorus allocation varies less than carbon allocation over the day–night cycle (Fig. 2g–n). An exception is ads-P, only detected in the dark period (Fig. 2o). Phosphorus allocation to polyphosphate is also higher in the light period but not significantly (Fig. 2n).

Discussion

The C : N of *Crocosphaera* in this study is in the typical range for many phytoplankton, but C : P and N : P are extraordinarily low under 50 μM phosphate, primarily due to the polyphosphate accumulation (Fig. 2) and secondarily due to high DNA content, indicative of an accumulation of multiple copies of the genome (Supporting Information Table S6). Polyploidy is common in cyanobacteria, including *Synechococcus* (Binder and Chisholm 1990), *Synechocystis* (Griese et al. 2011), *Anabaena* (Simon 1977), and *Trichodesmium* (Sargent et al. 2016), and in some cases has been related to growth phase and environmental factors (Watanabe 2020). The controls on

Fig. 1. Cell dimensions, cellular elemental density, and elemental ratios for two size phenotype strains of *Crocosphaera* (**subpanels 1**) at the end of the dark and the light period under 50 μM phosphate and (**subpanels 2**) under 0.5 μM phosphate. (**a**) cell diameter, (**b**) cell volume, (**c**) surface area to volume ratio, (**d**) carbon density, (**e**) nitrogen density, (**f**) phosphorus density, (**g**) C : N, (**h**) N : P, and (**i**) C : P. Error bars stand for 1 SDs from the average. Different letters above the bars in panels 1 denote a significant difference ($p < 0.05$) after two-way ANOVA (Supporting Information Table S4); (**h**1, **i**1) when the effect of phenotype × photoperiod interaction is significant ($p < 0.05$), only comparison between the photoperiods in WH0005 was assessed. Asterisks above the bar denote (I1) a significant difference from another photoperiod in WH0005 under 50 μM phosphate and denote (**subpanels 2**) a significant difference from another strain under 0.5 μM phosphate (Supporting Information Table S5). *$p < 0.05$; **$p < 0.01$; ***$p < 0.001$.

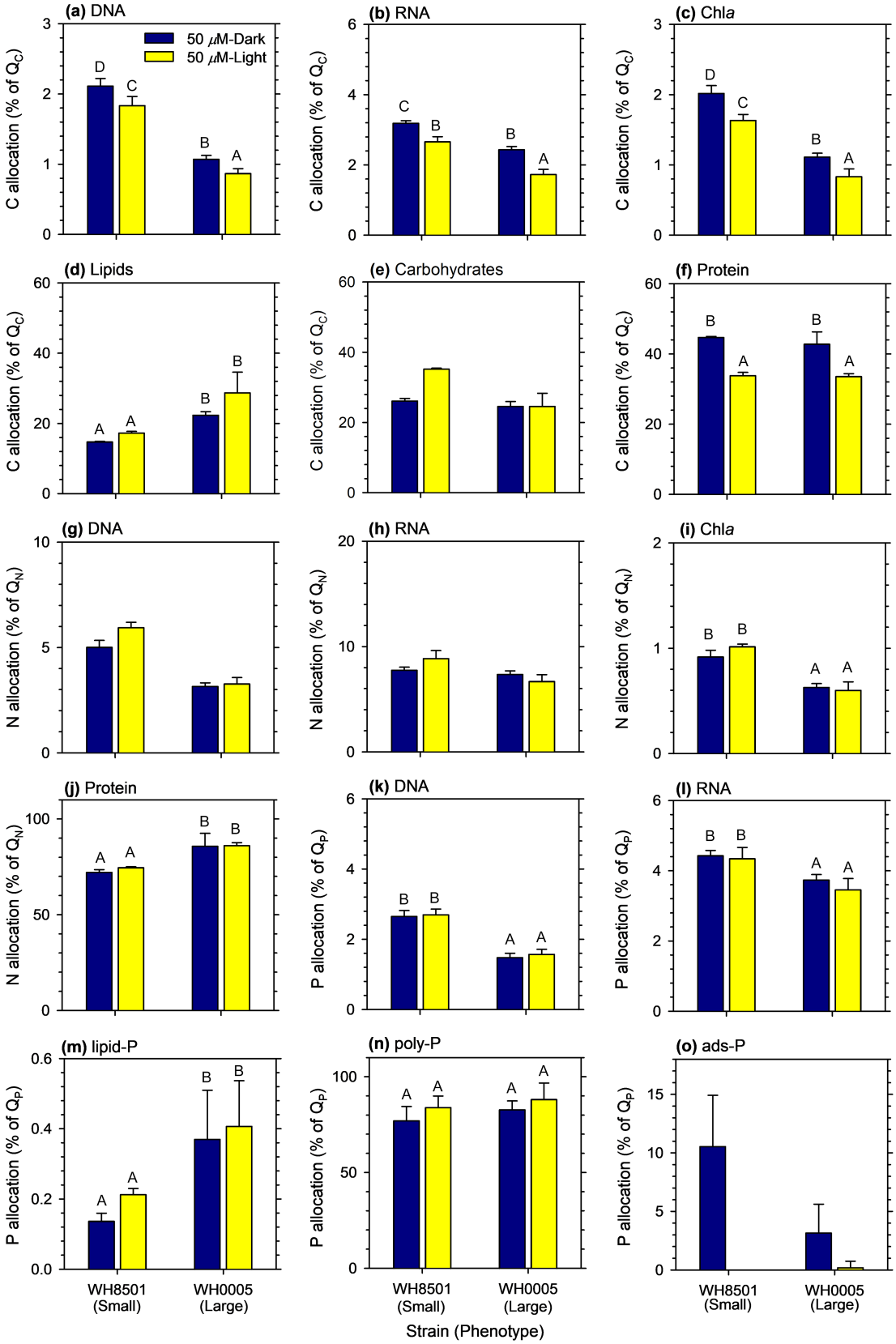

Fig. 2. Legend on next page.

polyphosphate in cyanobacteria are not well understood, but here we find a decrease in phosphate to 0.5 μM results in a C : N : P of 335 : 41 : 1 in WH8501 and 483 : 64 : 1 in WH0005, suggesting very low N : P due to high polyphosphate accumulation may not be common in the field when phosphate concentration is below 0.5 μM. A summary of N : P from experiments on *Crocosphaera* and the colonial diazotroph *Trichodesmium* further supports the hypothesis that polyphosphate accumulates under high phosphate concentrations, resulting in low N : P while low phosphate leads to higher N : P in nitrogen-fixing cyanobacteria (Table 1). Excluding polyphosphate and considering only phosphorus from RNA, lipids, and a single genome copy, the estimated N : P ratios under high-phosphate treatment were 44 for WH8501 and 49 for WH0005, closely matching those under low phosphate treatment. This further supports the hypothesis that low N : P in nitrogen-fixing cyanobacteria is due to the luxury P accumulation as polyphosphate and DNA.

The daily cycle of nitrogen fixation at night and oxygenic photosynthesis during the day drives a macromolecular remodeling of the cell in the service of maintaining nitrogenase and oxygen and energy management. The carbon and nitrogen dynamics have been well studied in *Crocosphaera*, although some of the phenotype differences have not been resolved and little is known about diel phosphorus management (Dron, Rabouille, Claquin, Chang, et al. 2012; Dron, Rabouille, Claquin, Le Roy, et al. 2012; Masuda et al. 2018; Shi et al. 2010). The C-rich macromolecules carbohydrates (WH8501) and lipids (WH0005) accumulate during the light period due to photosynthesis and then decline over the night period due to respiration (Dron, Rabouille, Claquin, Chang, et al. 2012), resulting in a 24% variation in C : N. The decline in carbon over the dark period is consistent with high respiratory requirements to manage oxygen to reduce nitrogenase inactivation (Inomura, Deutsch, et al. 2019). Großkopf and LaRoche (2012) estimate that under normal O_2 concentration, about 60% of the energetic cost of nitrogen fixation in *Crocosphaera* is due to the indirect costs of oxygen removal and nitrogenase synthesis to replace enzymes damaged by oxygen. An increase in cellular protein content in the dark period is due to the accumulation of fixed nitrogen into protein, phycobilins, and cyanophycin stores (Supporting Information Note S2), and related enzymes including nitrogenase and cyanophycin synthetase (Dron, Rabouille, Claquin, Chang, et al. 2012; Masuda et al. 2018). Diel changes in total cellular P are minor, with the largest shifts in polyphosphate and surface ads-P (Figs. 1, 2). These results suggest polyphosphate may play a role in energy management as the cell shifts from photosynthesis during the day to nitrogen fixation at night. The large polyphosphate stores are reduced in the dark and are possibly being used as a source of reductant. Surface ads-P accumulates in the dark and was undetectable at the end of the light period, consistent with the cell diverting energy away from P uptake during the night (Lin et al. 2016).

The two phenotypes of *Crocosphaera* studied here differ in cell volume by a factor of almost 2. C : N is significantly higher in the larger phenotype while N : P and C : P are not different across the phenotypes (Supporting Information Table S4). These differences in C : N may be a consequence of size-related costs associated with oxygen management or pigment packaging. The small-cell phenotype WH8501 has a 20% higher $SA : V$ than the large-cell WH0005. As a consequence, WH8501 will have a higher rate of O_2 diffusion into the cell, and therefore higher respiratory costs associated with oxygen management (Inomura, Deutsch, et al. 2019). We did not measure respiration rate in this experiment, but the diel change in total particulate carbon is approximately 110 and 150 fmol C cell^{-1} for WH8501 and WH0005, respectively (Supporting Information Table S4). While the magnitude of C loss over the day is similar for both phenotypes, it is a much larger percentage of cellular carbon in the small-cell (22%) compared to the large-cell phenotype (13%). During the light period, the increase in cellular carbon was mainly attributable to elevated carbohydrate levels in WH8501 and elevated lipid levels in WH0005. Carbohydrates are more readily metabolized than lipids, but lipids are higher-density energy storage molecules. The larger increase in lipids in the light period in WH0005 might be due to an increase in thylakoid membranes that minimize pigment packaging to improve photosynthetic efficiency, as observed in *Synechococcus* (Huokko et al. 2021), or to manage oxygen transmission within the cell (Inomura, Deutsch, et al. 2019). Transmission electron micrographs indicate *Crocosphaera* possesses multiple thylakoid membranes arranged in sinuous parallel clusters with starch granules held between the clusters (Dron, Rabouille, Claquin, Chang, et al. 2012; Inomura, Deutsch, et al. 2019; Masuda et al. 2024). Past work on *Crocosphaera* has found high rates of extracellular polymeric substance production (Bench et al. 2013; Sohm et al. 2011); $\sim$ 10% of total cellular carbon is excreted daily in WH8501 under a light intensity of 130 μmol quanta m^{-2} s^{-1} (Dron, Rabouille, Claquin, Chang, et al. 2012). Bacterial respiration of extracellular polymeric

Fig. 2. Comparisons of cellular (**a**–**f**) C, (**g**–**j**) N, and (**k**–**o**) P allocations (in percentage of the elemental quota) to (**a**, **g**, **k**) DNA, (**b**, **h**, **l**) RNA, (**c**, **i**) chlorophyll *a*, (**d**) lipids, (**e**) carbohydrates, (**f**, **j**) protein, (**m**) lipids-associated P, (**n**) polyphosphate, and (**o**) surface adsorbed P between *Crocosphaera* strains (WH8501 vs. WH0005) and between photoperiods (dark vs. light) in the experiment under 50 μM phosphate. Error bars stand for 1 SDs from the average. Upper-cased letters above the bars denote a significant difference ($p < 0.05$) (Supporting Information Table S8); (**e**, **g**–**h**, **o**) when the effect of phenotype $\times$ photoperiod interaction is significant ($p < 0.05$), only comparison between the photoperiods in WH0005 was assessed (the differences were not significant, $p > 0.05$).

Table 1. Cellular C, N, and P quotas (Q_C, Q_N, Q_P, fmol cell^{-1} or pmol trichome^{-1}) and ratios of *Crocosphaera* and *Trichodesmium* strains under different dissolved phosphorus concentrations (μM) in laboratory cultures or field samples (for *Trichodesmium* only) from the literature.

Strain/region	$[PO_4^{3-}]$	Q_C	Q_N	Q_P	C : N	N : P	C : P	References
Small-cell *Crocosphaera*								
WH8501	50	482	64	34.5	7.47	1.85	16.4	This study
	50	—	—	—	6.86	—	—	Dron, Rabouille, Claquin, Le Roy, et al. (2012)
	50*	527	67.2	7.71	7.84	8.72	68.4	Rabouille et al. (2022)
	50	481	68.5	7.17	7.02	9.55	67.1	Rabouille et al. (2022)
	10	0.28	—	—	6.9	18.8	130	Fu et al. (2008)
	1	180	34	0.98	5.3	34.8	183	Knapp et al. (2012)
	0.5	220	36	1.1	6.1	31.7	189	Knapp et al. (2012)
	0.5	424	50.8	1.27	8.31	40.6	335	This study
WH0401	10	—	—	—	7.3	20.8	152	Fu et al. (2014)
Large-cell *Crocosphaera*								
PS0609	20	667	61.1	41.3	11.0	1.5	16.2	Masuda et al. (2013)
WH0005	50	1117	127	68.8	8.84	1.88	13.9	This study
	10	—	—	—	7.9	20.8	164	Fu et al. (2014)
	10	—	—	—	7.3–9.7	16	—	Zhu et al. (2020)
	0.5	—	—	—	8.1–9	22.5–25.4	—	Zhu et al. (2020)
	0.5	1160	158	2.50	7.35	64.0	483	This study
WH0003	10	—	—	—	7.2	20.6	148	Fu et al. (2014)
	10	1250	170	46	7.31	3.41	24.9	Liu et al. (2020)
	10†	1080	160	34	6.89	4.79	33.0	Liu et al. (2020)
	10‡	1070	150	9	7.00	17.9	125	Liu et al. (2020)
	10‖	1260	170	9	7.31	18.7	137	Liu et al. (2020)
	0.1	590	100	4	6.04	25.5	154	Liu et al. (2020)
WH0402	10	—	—	—	8.0	21.6	173	Fu et al. (2014)
Trichodesmium								
IMS101	50*	—	—	—	—	4.37–23.9	—	Mulholland et al. (2002)
	3*	—	—	—	—	23.8–156	—	Mulholland et al. (2002)
	1*	—	—	—	—	23.6–140	—	Mulholland et al. (2002)
	50	—	—	—	—	7–18	—	Krauk et al. (2006)
	5	—	—	—	—	37–140	—	Krauk et al. (2006)
	1	424	65.5	2.0	6.2	34.7	209	Knapp et al. (2012)
	0.5	410	76.6	2.0	5.1	49.5	234	Knapp et al. (2012)
	0.5	1342	—	0.97–4.84	8.56	30.1–93.8	—	White et al. (2006)
	10	—	—	—	5.3–6.3	14.1–14.7	—	Zhu et al. (2020)
	0.5	—	—	—	6–7	53–58	—	Zhu et al. (2020)
GBR	10	—	—	—	4.5–6.5	19.7–20.9	—	Zhu et al. (2020)
	0.5	—	—	—	6–8	41.1–50.1	—	Zhu et al. (2020)
KO4-20	10	—	—	—	6.9	20.4	141	Fu et al. (2014)
RLI	10	—	—	—	6.4	19.5	125	Fu et al. (2014)
21-75	10	—	—	—	6.5	20.4	133	Fu et al. (2014)
Subtropical NA	—	—	—	—	—	14–30	—	Sañudo-Wilhelmy et al. (2001)
Tropical NA	—	—	—	—	—	35–61	—	Sañudo-Wilhelmy et al. (2001)
NA	~ 0.03	—	—	—	—	43.5	—	Krauk et al. (2006)
Sargasso Sea	< 0.05§	—	—	—	—	32.9–110	185–623	Orchard et al. (2010)
GOM, floaters	—	—	—	—	—	49.9	—	Krauk et al. (2006)
GOM, sinkers	—	—	—	—	—	89.5	—	Krauk et al. 2006

(Continues)

Table 1. Continued

Strain/region	$[PO_4^{3-}]$	Q_C	Q_N	Q_P	C : N	N : P	C : P	References
North Pacific	< 0.11	—	—	—	—	36.2–40.1	—	Krauk et al. (2006)
Australian	< 0.3	—	—	—	—	22.4	—	Krauk et al. (2006)

Laboratory data are cited as incubation temperature was between 24°C and 28°C.
NA, North Atlantic; GOM, Gulf of Mexico.
*DOP only.
†Under 0.2 μM Al.
‡Phosphate deficiency was induced by 2 μM Al.
‖Phosphate deficiency was induced by 20 μM Al.
§DOP + DIP.

substance could reduce oxygen concentrations around *Crocosphaera*, although heterotrophic bacteria counts were low in this experiment. Furthermore, the relatively low particulate carbohydrate content of WH0005 vs. WH8501 may be a consequence of different levels of carbohydrate exudation vs. biosynthetic incorporation.

Cell size generally has a strong effect on nutrient affinity and demand. In this study, the phenotypes had very different responses to a decrease in phosphate from 50 to 0.5 μM. The small-cell phenotype WH8501 decreases cell volume, reducing resource requirements and increasing its $SA : V$ and thus its nutrient acquisition capacity. As its volume decreases, cellular C remains approximately constant and cellular N decreases, resulting in an increase in C : N while the opposite pattern is exhibited in the larger phenotype. N : P and C : P both increase greatly following the reduction in phosphate concentration in both phenotypes, but the larger phenotype exhibits a larger increase in both N : P and C : P (Fig. 1). The increase in $SA : V$ in the smaller phenotype would further increase oxygen diffusion rates; perhaps its elevated allocation of C and N to photosynthetic (Chl*a*) and biosynthetic (RNA) machinery (Fig. 2) increases anabolic capacity to ameliorate the higher respiratory requirements. These acclimation strategies suggest that the smaller phenotype is better adapted to lower nutrient environments, such as the upper water column in the oligotrophic subtropics (Bench et al. 2016; Wilson et al. 2017). The effect of cell size and associated biochemical and physiological differences on *Crocosphaera* biogeography and nitrogen fixation potential should be considered when modeling responses of nitrogen fixers to changing environmental conditions.

The influence of N : P variability in nitrogen-fixing cyanobacteria for global nitrogen fixation and the biogeography of diazotrophs has yet to be assessed. Under a variable nutrient regime, an enhanced P storage capacity by *Crocosphaera*, and other diazotrophs such as *Trichodesmium*, provides a mechanism to increase their competitiveness for phosphate and therefore might facilitate enhanced ocean nitrogen fixation. Model experiments have examined N-storage capacity in *Crocosphaera* but P-storage has as yet been neglected (Inomura, Masuda, et al. 2019). Field measurements indicate in the upper 0–150 m of the North Pacific Subtropical Gyre around 16–44% of total particulate phosphorus associated with bulk planktonic matter may be polyphosphate (Diaz et al. 2016). The role of polyphosphate in phytoplankton biology and ecology and biogeochemistry is not well understood. It has been hypothesized that in addition to being a P store, it may be an energy store and biochemical buffer for ATP and DNA replication (Kornberg et al. 1999). In bacteria, polyphosphate reduces mortality in responses to some stressors (Brown and Kornberg 2004). Here we found that the growth of *Crocosphaera* was reduced under high-phosphate conditions with elevated cellular phosphorus and polyphosphate, consistent with an energetic cost of polyphosphate accumulation. Much more needs to be learned from laboratory experiments, field observations, and models to explore the causes and extent of stoichiometric variability in nitrogen fixers.

Author Contributions

Sing-how Tuo, Ying-Yu Hu, Andrew J. Irwin, and Zoe V. Finkel contributed to the conceptualization. Sing-how Tuo and Ying-Yu Hu performed the investigation. Sing-how Tuo and Andrew J. Irwin contributed to formal analysis and visualization. Sing-how Tuo prepared the original draft. Zoe V. Finkel, Andrew J. Irwin, Michael J. Follows, and Ying-Yu Hu contributed to the review and editing.

Acknowledgments

We thank Dr. Jon Zehr for providing the *Crocosphaera* strains, Dr. Suchandan Bemal, Dr. Nuwanthi Samarasinghe, and Gracie Walker for their assistance with sample collection as well as Dr. Doug Wallace, Claire Normandeau, and Anadiuska Rondon for their assistance with CHN and dissolved nutrient analysis. This work was supported by the Simons Foundation (The Simons Collaboration on Computational Biogeochemical Modeling of Marine Ecosystems (CBIOMES), Grant 549935 to Andrew J. Irwin and 549937 to Zoe V. Finkel; (The Simons Collaboration on Ocean Processes and Ecology) SCOPE-Gradients, Grant 723789 to Zoe V. Finkel and Grant 721235 to Andrew J. Irwin), the Canada Research Chairs Program, and The Natural Sciences and Engineering Research Council of Canada (NSERC).

Conflicts of Interest

None declared.

Data Availability Statement

The data that support the findings of this study are available from the corresponding author upon reasonable request.

References

Benavides, M., M. Caffin, S. Duhamel, et al. 2022. "Anomalously High Abundance of *Crocosphaera* in the South Pacific Gyre." *FEMS Microbiology Letters* 369: fnac039. https://doi.org/10.1093/femsle/fnac039.

Bench, S. R., I. Frank, J. Robidart, and J. P. Zehr. 2016. "Two Subpopulations of *Crocosphaera watsonii* Have Distinct Distributions in the North and South Pacific." *Environmental Microbiology* 18: 514–524. https://doi.org/10.1111/1462-2920.13180.

Bench, S. R., P. Heller, I. Frank, M. Arciniega, I. N. Shilova, and J. P. Zehr. 2013. "Whole Genome Comparison of Six *Crocosphaera watsonii* Strains with Differing Phenotypes." *Journal of Phycology* 49: 786–801. https://doi.org/10.1111/jpy.12090.

Berdalet, E., C. Roldán, and M. P. Olivar. 2005. "Quantifying RNA and DNA in Planktonic Organisms with SYBR Green II and Nucleases. Part B. Quantification in Natural Samples." *Scientia Marina* 69: 17–30. https://doi.org/10.3989/scimar.2005.69n117.

Binder, B. J., and S. W. Chisholm. 1990. "Relationship Between DNA Cycle and Growth Rate in *Synechococcus* Sp. Strain PCC 6301." *Journal of Bacteriology* 172: 2313–2319. https://doi.org/10.1128/jb.172.5.2313-2319.1990.

Brown, M. R., and A. Kornberg. 2004. "Inorganic Polyphosphate in the Origin and Survival of Species." *Proceedings of the National Academy of Sciences of the United States of America* 101: 16085–16087. https://doi.org/10.1073/pnas.0406909101.

Chen, P. S., T. Y. Toribara, and H. Warner. 1956. "Microdetermination of Phosphorus." *Analytical Chemistry* 28: 1756–1758. https://doi.org/10.1021/ac60119a033.

Chen, Y. B., J. P. Zehr, and M. Mellon. 1996. "Growth and Nitrogen Fixation of the Diazotrophic Filamentous Nonheterocystous Cyanobacterium *Trichodesmium* Sp. IMS 101 in Defined Media: Evidence for a Circadian Rhythm." *Journal of Phycology* 32: 916–923. https://doi.org/10.1111/j.0022-3646.1996.00916.x.

Diaz, J. M., K. M. Björkman, S. T. Haley, et al. 2016. "Polyphosphate Dynamics at Station ALOHA, North Pacific Subtropical Gyre." *Limnology and Oceanography* 61: 227–239. https://doi.org/10.1002/lno.10206.

Dron, A., S. Rabouille, P. Claquin, B. Le Roy, A. Talec, and A. Sciandra. 2012. "Light–Dark (12:12) Cycle of Carbon and Nitrogen Metabolism in *Crocosphaera watsonii* WH8501: Relation to the Cell Cycle." *Environmental Microbiology* 14: 967–981. https://doi.org/10.1111/j.1462-2920.2011.02675.x.

Dron, A., S. Rabouille, P. Claquin, et al. 2012. "Light: Dark (12: 12 h) Quantification of Carbohydrate Fluxes in *Crocosphaera watsonii*." *Aquatic Microbial Ecology* 68: 43–55. https://doi.org/10.3354/ame01600.

Dutkiewicz, S., B. Ward, F. Monteiro, and M. Follows. 2012. "Interconnection of Nitrogen Fixers and Iron in the Pacific Ocean: Theory and Numerical Simulations." *Global Biogeochemical Cycles* 26: GB1012. https://doi.org/10.1029/2011GB004039.

Fagerbakke, K. M., M. Heldal, and S. Norland. 1996. "Content of Carbon, Nitrogen, Oxygen, Sulfur and Phosphorus in Native Aquatic and Cultured Bacteria." *Aquatic Microbial Ecology* 10: 15–27. https://doi.org/10.3354/ame010015.

Falkowski, P. G. 1997. "Evolution of the Nitrogen Cycle and its Influence on the Biological Sequestration of CO_2 in the Ocean." *Nature* 387: 272–275. https://doi.org/10.1038/387272a0.

Fu, F.-X., E. Yu, N. S. Garcia, et al. 2014. "Differing Responses of Marine N_2 Fixers to Warming and Consequences for Future Diazotroph Community Structure." *Aquatic Microbial Ecology* 72: 33–46. https://doi.org/10.3354/ame01683.

Fu, F.-X., M. R. Mulholland, N. S. Garcia, et al. 2008. "Interactions between Changing pCO_2, N_2 Fixation, and Fe Limitation in the Marine Unicellular Cyanobacterium *Crocosphaera*." *Limnology and Oceanography* 53: 2472–2484. https://doi.org/10.4319/lo.2008.53.6.2472.

Geider, R. J., and J. La Roche. 2002. "Redfield Revisited: Variability of C:N:P in Marine Microalgae and its Biochemical Basis." *European Journal of Phycology* 37: 1–17. https://doi.org/10.1017/S0967026201003456.

Griese, M., C. Lange, and J. Soppa. 2011. "Ploidy in Cyanobacteria." *FEMS Microbiology Letters* 323: 124–131. https://doi.org/10.1111/j.1574-6968.2011.02368.x.

Großkopf, T., and J. LaRoche. 2012. "Direct and Indirect Costs of Dinitrogen Fixation in *Crocosphaera watsonii* WH8501 and Possible Implications for the Nitrogen Cycle." *Frontiers in Microbiology* 3: 236. https://doi.org/10.3389/fmicb.2012.00236.

Hu, Y.-Y., A. J. Irwin, and Z. V. Finkel. 2022. "Improving Quantification of Particulate Phosphorus." *Limnology and Oceanography: Methods* 20: 729–740. https://doi.org/10.1002/lom3.10517.

Hu, Y.-Y., A. J. Irwin, and Z. V. Finkel. 2024. "An Improved Method to Quantify Bulk Carbohydrate in Marine Planktonic Samples." *Limnology and Oceanography: Methods* 22: 399–415. https://doi.org/10.1002/lom3.10614.

Hu, Y.-Y., and Z. V. Finkel. 2022. "Lipids in Microalgae: Quantitation by Acid-Dichromate Method in Microtiter Plate V.2." *Protocols.io*. doi:https://doi.org/10.17504/protocols.io.e6nvw9dpzgmk/v2.

Hu, Y.-Y., and Z. V. Finkel. 2023a. "DAPI-Based Polyphosphate Estimation With Extraction Sufficiency Validation: A Method for Quantifying Polyphosphate

From Microalgae Samples." *Protocols.io*. doi:https://doi.org/10.17504/protocols.io.ewov1ox87lr2/v1.

Hu, Y.-Y., and Z. V. Finkel. 2023b. "Estimate Phospholipids From Microalgae V.2." *Protocols.io* https://doi.org/10.17504/protocols.io.q26g74r19gwz/v2.

Hu, Y.-Y., and Z. V. Finkel. 2023c. "Total RNA and DNA From Microalgae (12 Samples per Microplate) V.11." *Protocols.io* https://doi.org/10.17504/protocols.io.6qpvro85bvmk/v11.

Hu, Y.-Y., C. Lord, and Z. V. Finkel. 2022a. "Chloroform-Methanol Protein Precipitation From Microalgae and Pierce BCA Assay." *Protocols.io*. doi:https://doi.org/10.17504/protocols.io.yxmvm2e25g3p/v1.

Hu, Y.-Y., C. Lord, and Z. V. Finkel. 2022b. "Total Crude Protein in Plankton: Pierce BCA Protein Assay (Including the Enhanced Assay for Low Biomass) V.3." *Protocols.io*. doi: https://doi.org/10.17504/protocols.io.5qpvoy5e7g4o/v3.

Huokko, T., T. Ni, G. F. Dykes, et al. 2021. "Probing the Biogenesis Pathway and Dynamics of Thylakoid Membranes." *Nature Communications* 12: 3475. https://doi.org/10.1038/s41467-021-23680-1.

Inomura, K., A. W. Omta, D. Talmy, J. Bragg, C. Deutsch, and M. J. Follows. 2020. "A Mechanistic Model of Macromolecular Allocation, Elemental Stoichiometry, and Growth Rate in Phytoplankton." *Frontiers in Microbiology* 11: 86. https://doi.org/10.3389/fmicb.2020.00086.

Inomura, K., C. Deutsch, S. T. Wilson, et al. 2019. "Quantifying Oxygen Management and Temperature and Light Dependencies of Nitrogen Fixation by *Crocosphaera watsonii*." *mSphere* 4: e00531-00519. https://doi.org/10.1128/mSphere.00531-19.

Inomura, K., T. Masuda, and J. M. Gauglitz. 2019. "Active Nitrogen Fixation by *Crocosphaera* Expands Their Niche Despite the Presence of Ammonium—A Case Study." *Scientific Reports* 9: 15064. https://doi.org/10.1038/s41598-019-51378-4.

Knapp, A. N., J. Dekaezemacker, S. Bonnet, J. A. Sohm, and D. G. Capone. 2012. "Sensitivity of *Trichodesmium erythraeum* and *Crocosphaera watsonii* Abundance and N_2 Fixation Rates to Varying NO_3^- and PO_4^{3-} Concentrations in Batch Cultures." *Aquatic Microbial Ecology* 66: 223–236. https://doi.org/10.3354/ame01577.

Kornberg, A., N. N. Rao, and D. Ault-Riché. 1999. "Inorganic Polyphosphate: A Molecule of Many Functions." *Annual Review of Biochemistry* 68: 89–125. https://doi.org/10.1146/annurev.biochem.68.1.89.

Krauk, J. M., T. A. Villareal, J. A. Sohm, J. P. Montoya, and D. G. Capone. 2006. "Plasticity of N: P Ratios in Laboratory and Field Populations of *Trichodesmium* Spp." *Aquatic Microbial Ecology* 42: 243–253. https://doi.org/10.3354/ame042243.

Lin, S., R. W. Litaker, and W. G. Sunda. 2016. "Phosphorus Physiological Ecology and Molecular Mechanisms in Marine Phytoplankton." *Journal of Phycology* 52: 10–36. https://doi.org/10.1111/jpy.12365.

Liu, J., L. Zhou, Z. Ke, G. Li, and Y. Tan. 2020. "Phosphorus Deficiency Induced by Aluminum in a Marine Nitrogen-Fixing Cyanobacterium *Crocosphaera watsonii* WH0003." *Chemosphere* 246: 125641. https://doi.org/10.1016/j.chemosphere.2019.125641.

Marie, D., N. Simon, and D. Vaulot. 2005. "Phytoplankton Cell Counting by Flow Cytometry." In Algal Culturing Techniques, edited by R. A. Anderson, 253–267. Elsevier.

Masuda, T., G. Bernát, M. Bečková, et al. 2018. "Diel Regulation of Photosynthetic Activity in the Oceanic Unicellular Diazotrophic Cyanobacterium *Crocosphaera watsonii* WH8501." *Environmental Microbiology* 20: 546–560. https://doi.org/10.1111/1462-2920.13963.

Masuda, T., J. Mareš, T. Shiozaki, K. Inomura, A. Fujiwara, and O. Prášil. 2024. "*Crocosphaera watsonii* – A Widespread Nitrogen-Fixing Unicellular Marine Cyanobacterium." *Journal of Phycology* 60: 604–620. https://doi.org/10.1111/jpy.13450.

Masuda, T., K. Furuya, T. Kodama, S. Takeda, and P. J. Harrison. 2013. "Ammonium Uptake and Dinitrogen Fixation by the Unicellular Nanocyanobacterium *Crocosphaera watsonii* in Nitrogen-Limited Continuous Cultures." *Limnology and Oceanography* 58: 2029–2036. https://doi.org/10.4319/lo.2013.58.6.2029.

Mills, M. M., and K. R. Arrigo. 2010. "Magnitude of Oceanic Nitrogen Fixation Influenced by the Nutrient Uptake Ratio of Phytoplankton." *Nature Geoscience* 3: 412–416. https://doi.org/10.1038/ngeo856.

Mulholland, M. R., S. Floge, E. J. Carpenter, and D. G. Capone. 2002. "Phosphorus Dynamics in Cultures and Natural Populations of *Trichodesmium* Spp." *Marine Ecology Progress Series* 239: 45–55. https://doi.org/10.3354/meps239045.

Myklestad, S. M., E. Skånøy, and S. Hestmann. 1997. "A Sensitive and Rapid Method for Analysis of Dissolved Mono- and Polysaccharides in Seawater." *Marine Chemistry* 56: 279–286. https://doi.org/10.1016/S0304-4203(96)00074-6.

Nayar, S., and L. M. Chou. 2003. "Relative Efficiencies of Different Filters in Retaining Phytoplankton for Pigment and Productivity Studies." *Estuarine, Coastal and Shelf Science* 58: 241–248. https://doi.org/10.1016/S0272-7714(03)00075-1.

Ni, G., G. Zimbalatti, C. D. Murphy, et al. 2017. "Arctic *Micromonas* Uses Protein Pools and Non-photochemical Quenching to Cope with Temperature Restrictions on Photosystem II Protein Turnover." *Photosynthesis Research* 131: 203–220. https://doi.org/10.1007/s11120-016-0310-6.

Orchard, E. D., C. R. Benitez-Nelson, P. J. Pellechia, M. W. Lomas, and S. T. Dyhrman. 2010. "Polyphosphate in *Trichodesmium* from the Low-Phosphorus Sargasso Sea." *Limnology and Oceanography* 55: 2161–2169. https://doi.org/10.4319/lo.2010.55.5.2161.

Pande, S., R. P. Khan, and T. Venkitasubramanian, 1963. "Microdetermination of Lipids and Serum Total Fatty Acids." *Analytical Biochemistry* 6: 415–423. https://doi.org/10.1016/0003-2697(63)90094-0.

Rabouille, S., L. Tournier, S. Duhamel, et al. 2022. "Organic Phosphorus Scavenging Supports Efficient Growth of Diazotrophic Cyanobacteria under Phosphate Depletion." *Frontiers in Microbiology* 13: 848647. https://doi.org/10.3389/fmicb.2022.848647.

Raven, J. A. 1994. "Why Are there no Picoplanktonic O_2 Evolvers with Volumes Less Than 10^{-19} m^3." *Journal of Plankton Research* 16: 565–580. https://doi.org/10.1093/plankt/16.5.565.

Saito, M. A., E. M. Bertrand, S. Dutkiewicz, et al. 2011. "Iron Conservation by Reduction of Metalloenzyme Inventories in the Marine Diazotroph *Crocosphaera watsonii*." *Proceedings of the National Academy of Sciences of the United States of America* 108: 2184–2189. https://doi.org/10.1073/pnas.1006943108.

Sañudo-Wilhelmy, S. A., A. B. Kustka, C. J. Gobler, et al. 2001. "Phosphorus Limitation of Nitrogen Fixation by *Trichodesmium* in the Central Atlantic Ocean." *Nature* 411: 66–69. https://doi.org/10.1038/35075041.

Sargent, E. C., A. Hitchcock, S. A. Johansson, et al. 2016. "Evidence for Polyploidy in the Globally Important Diazotroph *Trichodesmium*." *FEMS Microbiology Letters* 363: fnw244. https://doi.org/10.1093/femsle/fnw244.

Shi, T., I. Ilikchyan, S. Rabouille, and J. P. Zehr. 2010. "Genome-Wide Analysis of Diel Gene Expression in the Unicellular N_2-Fixing Cyanobacterium *Crocosphaera watsonii* WH 8501." *ISME Journal* 4: 621–632. https://doi.org/10.1038/ismej.2009.148.

Shoaf, W. T., and B. W. Lium. 1976. "Improved Extraction of Chlorophyll *a* and *b* From Algae Using Dimethyl Sulfoxide." *Limnology and Oceanography* 21: 926–928. https://doi.org/10.4319/lo.1976.21.6.0926.

Simon, R. D. 1977. "Macromolecular Composition of Spores From the Filamentous Cyanobacterium *Anabaena cylindrica*." *Journal of Bacteriology* 129: 1154–1155. https://doi.org/10.1128/jb.129.2.1154-1155.1977.

Sohm, J. A., B. R. Edwards, B. G. Wilson, and E. A. Webb. 2011. "Constitutive Extracellular Polysaccharide (EPS) Production by Specific Isolates of *Crocosphaera watsonii*." *Frontiers in Microbiology* 2: 229. https://doi.org/10.3389/fmicb.2011.00229.

Solórzano, L., and J. H. Sharp. 1980. "Determination of Total Dissolved Phosphorus and Particulate Phosphorus in Natural Waters." *Limnology and Oceanography* 25: 754–758. https://doi.org/10.4319/lo.1980.25.4.0754.

Sterner, R. W., and J. J. Elser. 2003. Ecological Stoichiometry: The Biology of Elements From Molecules to the Biosphere. Princeton University Press. https://doi.org/10.1515/9781400885695.

Tovar-Sanchez, A., S. A. Sañudo-Wilhelmy, M. Garcia-Vargas, R. S. Weaver, L. C. Popels, and D. A. Hutchins. 2003. "A Trace Metal Clean Reagent to Remove Surface-Bound Iron From Marine Phytoplankton." *Marine Chemistry* 82: 91–99. https://doi.org/10.1016/S0304-4203(03)00054-9.

Watanabe, S. 2020. "Cyanobacterial Multi-Copy Chromosomes and their Replication." *Bioscience, Biotechnology, and Biochemistry* 84: 1309–1321. https://doi.org/10.1080/09168451.2020.1736983.

Webb, E. A., I. M. Ehrenreich, S. L. Brown, F. W. Valois, and J. B. Waterbury. 2009. "Phenotypic and Genotypic Characterization of Multiple Strains of the Diazotrophic Cyanobacterium, *Crocosphaera watsonii*, Isolated From the Open Ocean." *Environmental Microbiology* 11: 338–348. https://doi.org/10.1111/j.1462-2920.2008.01771.x.

Weber, T., and C. Deutsch. 2014. "Local Versus Basin-Scale Limitation of Marine Nitrogen Fixation." *Proceedings of the National Academy of Sciences of the United States of America* 111: 8741–8746. https://doi.org/10.1073/pnas.1317193111.

Wilson, S. T., F. O. Aylward, F. Ribalet, et al. 2017. "Coordinated Regulation of Growth, Activity and Transcription in Natural Populations of the Unicellular Nitrogen-Fixing Cyanobacterium *Crocosphaera*." *Nature Microbiology* 2: 17118. https://doi.org/10.1038/nmicrobiol.2017.118.

Zehr, J. P., J. B. Waterbury, P. J. Turner, et al. 2001. "Unicellular Cyanobacteria Fix N_2 in the Subtropical North Pacific Ocean." *Nature* 412: 635–638. https://doi.org/10.1038/35088063.

Zhu, Z., F. Fu, P. Qu, et al. 2020. "Interactions between Ultraviolet Radiation Exposure and Phosphorus Limitation in the Marine Nitrogen-Fixing Cyanobacteria *Trichodesmium* and *Crocosphaera*." *Limnology and Oceanography* 65: 363–376. https://doi.org/10.1002/lno.11304.

Supporting Information

Additional Supporting Information may be found in the online version of this article.

Submitted 19 August 2025
Revised 17 February 2026
Accepted 18 July 2026